Critical Current Scaling in Long Diffusive Graphene-Based Josephson Junctions

Chung Ting Ke,[*,†] Ivan V. Borzenets,[‡] Anne W. Draelos,[†] Francois Amet,[†,¶] Yuriy Bomze,[†] Gareth Jones,[§] Monica Craciun,[§] Saverio Russo,[§] Michihisa Yamamoto,[‡] Seigo Tarucha,[‡,∥] and Gleb Finkelstein[*,†]

[†]Department of Physics, Duke University, Durham, North Carolina 27708, United States
[‡]Department of Applied Physics, The University of Tokyo, Tokyo 113-8654, Japan
[¶]Department of Physics, Appalachian State University, Boone, North Carolina 28608, United States
[§]College of Engineering, Mathematics and Physical Sciences, University of Exeter, Exeter, Devon EX4, United Kingdom
[∥]RIKEN, Center for Emergent Matter Science, Tokyo 351-0198, Japan

Ⓢ Supporting Information

ABSTRACT: We present transport measurements on long, diffusive, graphene-based Josephson junctions. Several junctions are made on a single-domain crystal of CVD graphene and feature the same contact width of ~ 9 μm but vary in length from 400 to 1000 nm. As the carrier density is tuned with the gate voltage, the critical current in these junctions ranges from a few nanoamperes up to more than 5 μA, while the Thouless energy, E_{Th}, covers almost 2 orders of magnitude. Over much of this range, the product of the critical current and the normal resistance $I_C R_N$ is found to scale linearly with E_{Th}, as expected from theory. However, the value of the ratio $I_C R_N / E_{Th}$ is found to be 0.1–0.2, which much smaller than the predicted ~ 10 for long diffusive SNS junctions.

KEYWORDS: Graphene, superconductivity, Josephson junction, diffusive SNS junction, Thouless energy
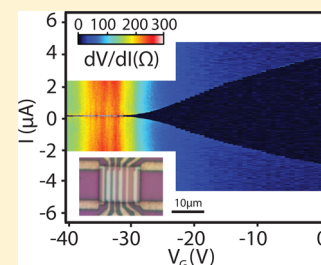
Electrical current can flow without dissipation through a normal (nonsuperconducting) material connected to superconducting contacts.[1] Using graphene as a normal region, one can create gate-tunable superconducting devices which feature both a high electronic mobility and a large Fermi velocity.[2–5] As a result, in the cleanest devices supercurrents can propagate ballistically on a micron scale.[6–8] However, the mechanism allowing supercurrent transport through diffusive graphene is not yet fully understood. Even in relatively disordered samples, supercurrents can propagate through channel lengths exceeding one micron; however, the channel length dependence of the critical current has not yet been explored.

Conventional theory for diffusive superconductor–normal metal-superconductor (SNS) junctions predicts that the critical current of the junction (I_C) is determined by the Thouless energy $E_{Th} = \hbar D / L^2$, where D is the diffusion coefficient and L is the channel length. For long junctions where $E_{Th} \ll \Delta$, I_C is predicted to be given by $e I_C R_N \approx 10 E_{Th}$.[9] Here, Δ is the superconducting gap in the leads, and R_N is the normal state resistance of the junction. In this work, we investigate the relationship between $I_C R_N$ and E_{Th} in Josephson junctions of different lengths made on the same graphene crystal. We establish that in a wide range of critical currents (covering more than 2 orders of magnitude) and densities away from the Dirac point, $I_C R_N$ is indeed proportional to E_{Th}. However, the coefficient of proportionality is significantly suppressed compared to the expected value of ~ 10.

Our devices utilize large domain size (~ 100 μm) graphene grown via chemical vapor deposition (CVD).[10–14] A macroscopic piece of graphene film, grown on copper foil,[10] is transferred to a 300 nm oxide SiO_2/Si substrate using the standard PMMA/$FeCl_3$ transfer technique.[12] The superconducting contacts are made by depositing 120 nm of lead (Pb) on top of a 6 nm Pd sticking layer, which provides an electrically transparent contact to graphene. Pb has a high critical temperature $T_C \sim 7$ K so that a supercurrent can be observed through graphene junctions at temperatures up to 4 K.[15,16] Our three junctions have lengths (distance between the contacts) of $L = 400$, 600, and 1000 nm [Figure 1a]. The width of the contacts is $W = 9$ μm, which yields a sufficiently high supercurrent even for the longest junction. The junctions are isolated from the bonding pads by on-chip resistors in the range of 500 Ω to a few kΩ placed just outside the junctions. These resistors are created by partially oxidizing the Pb contact outside of the junctions using oxygen plasma. The CVD graphene is not encapsulated, suspended, or annealed; the resulting electron mean free path is less than 100 nm, as estimated from the bulk resistance. Thus, the devices are definitely in the diffusive junction limit.[9]

The measurements are performed in a dilution refrigerator with a base temperature of 50 mK. The device is isolated via low temperature RC filters, resistive coaxial lines, and RF
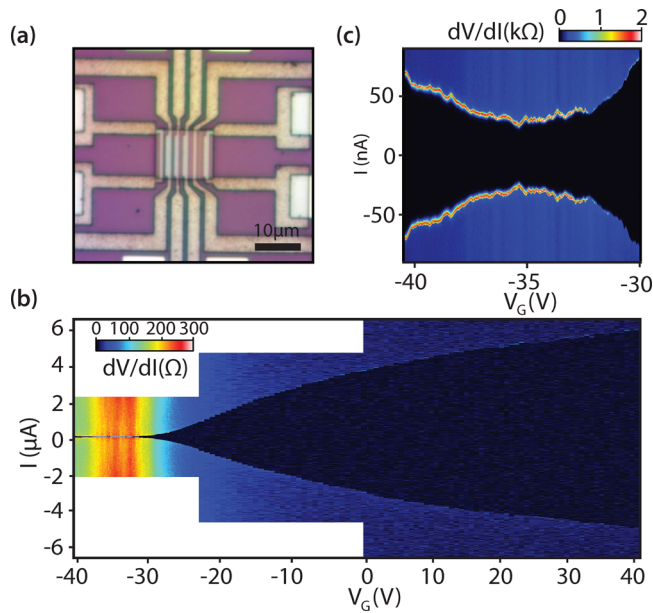
(a)

10μm

(c) dV/dI(kΩ) 0 1 2

(b)

Figure 1. (a) Optical microscope image of the graphene-based Josephson junction device. A 9×20 μm active area is defined in CVD graphene and the unused material is etched away. Josephson junctions of the same width, but varying lengths (400, 600, 1000, 1500, and 2000 nm) are made by depositing superconducting metal contacts onto the graphene. In order to form resistors that isolate the junctions from the rest of the circuit, parts of electrodes located away from the active area are oxidized with oxygen plasma. Only the first three junctions are used in this work. (b) Differential resistance dV/dI measured versus applied current and gate voltage in the 400 nm junction. The full backgate range from 40 to -40 V is divided into three separate maps with different current ranges. The superconducting region is observed around zero current (dark region of vanishing resistance.) The current is swept from negative to positive bias. I_R, the retrapping current from the normal to the superconducting state (observed at negative current) is smaller but comparable to I_S, the switching current from the superconducting to the normal state (at positive current.) (c) Zoomed-in resistance map around the Dirac point.

shielding. Our previous measurements using the same system have shown the electron temperature to be close to the lattice temperature. In particular, switching currents on a nano-amperes scale have been reliably measured.[8] Figure 1b shows the differential resistance dV/dI map measured versus the applied current I and the back-gate voltage V_G for the 400 nm device. The area of zero resistance (black region) indicates the superconducting regime, which persists for all values of the gate voltage. In this measurement, the current is swept from negative to positive; thus, at negative bias the device transitions from the normal to the superconducting state, yielding the retrapping current I_R. At positive current, the junction switches from the superconducting to the normal state at the switching current I_S, which is greater, but comparable to I_R.[1]

We have previously studied the hysteretic $I-V$ curves in graphene junctions that were engineered to be overdamped.[17] As opposed to the underdamped junctions, the origin of hysteresis was found to be overheating.[18] Regardless of the nature of the junction dynamics, statistical analysis of the switching currents performed in the current work shows that the true critical current I_C is only 20% larger than the switching current I_S (see the Supporting Information for a representative

histogram). Therefore, in the following we use the measured switching currents to represent I_C.

Figure 1c shows a high resolution dV/dI map measured around the Dirac point (DP), where the switching current I_S is the lowest. The DP in this junction is located at $V_G = -35$ V, and the DPs in other junctions are located within 3 V of this value, indicating that our graphene is uniformly N-doped. In the following, we plot the voltage as measured from the Dirac point, $V_G - V_D$. Figure 2a,b shows the normal resistance R_N and the switching current I_S versus V_G for all three junctions. (R_N is measured at bias currents much greater than the switching current.) Naturally, the switching current decreases with increasing channel length. The minimum I_S measured at the Dirac point is ~25 nA for the 400 nm junction and drops to ~6 nA for the 1000 nm junction. Because these small values are strongly affected by fluctuations, we exclude them from the further analysis.

In long diffusive SNS junctions, the product of the critical current and normal resistance $I_C R_N$ is expected to be proportional to $E_{Th} \ll \Delta$.[9] The Thouless energy $E_{Th} = \hbar D/L^2$ can be further expressed as a function of conductivity σ, and the density of states $\partial n/\partial \varepsilon$. The conductivity could be obtained from R_N as $\sigma = L/(R_N - R_C)W$, where W is the width of the junction and R_C is the contact resistance. R_C for each junction can be fitted by relying on the fact that σ of diffusive graphene scales linearly with gate voltage measured from the Dirac point, so that $1/(R_N - R_C)$ should be $\propto (V_G - V_D)$.[19] The resulting R_C values for the three junctions are found to be in the range of ~6−14 Ω. The Thouless energy may be eventually rewritten as

$$E_{Th} = \frac{\hbar\sigma}{e^2 L^2}\left(\frac{\partial \varepsilon}{\partial n}\right) \propto \frac{1}{(R_N - R_C)LW\sqrt{n}} \tag{1}$$

where $n \equiv C(V_G - V_D)/e$ is the carrier density and C is the gate capacitance.

Figure 2c shows the resulting dependence of the Thouless energy on V_G, as calculated from eq 1. Around the neutrality point, the carrier density is inhomogeneous and fluctuates strongly in space.[20] In this regime, the calculation of E_{Th} becomes invalid resulting in a fictitious peak at $V_G = V_D$; the very low density regime is therefore excluded from future analysis. For a junction to be in the regime where $I_C R_N \propto E_{Th}$, the Thouless energy must be much larger than $k_B T$ but smaller than the superconducting gap Δ. These conditions hold for a wide range of densities in all three junctions since $k_B T \sim 4.3$ μeV for $T = 50$ mK and the superconducting gap of Pb is 1.3 meV. This gap is not expected to be greatly reduced by a normal metal (Pd) sticking layer which is less than 10 nm thick.[21]

Finally, Figure 2d shows the product of $I_C R_N$ for the same junction. We expect the relation between the critical current and the Thouless energy to be of the form $eI_C R_N = \alpha E_{Th}$ and indeed the shapes of the curves in Figure 2c,d are similar except in the vicinity of the DP. We further plot I_C as a function of the E_{Th}/R_N ratio in Figure 3. We find that the data measured from the three junctions of different lengths over more than 2 orders of magnitude in I_S collapse on the same linear curve, which is in agreement with the theory for diffusive SNS junctions.[9]

However, we find that the ratio $\alpha \equiv eI_C R_N/E_{Th} \sim 0.1-0.2$ is suppressed by a factor of 50−100 compared to the expected value of $\alpha \approx 10$, which has been observed in conventional metal SNS junctions.[9,22] It is possible that the special nature of graphene can result in the suppression of the critical current.[23]
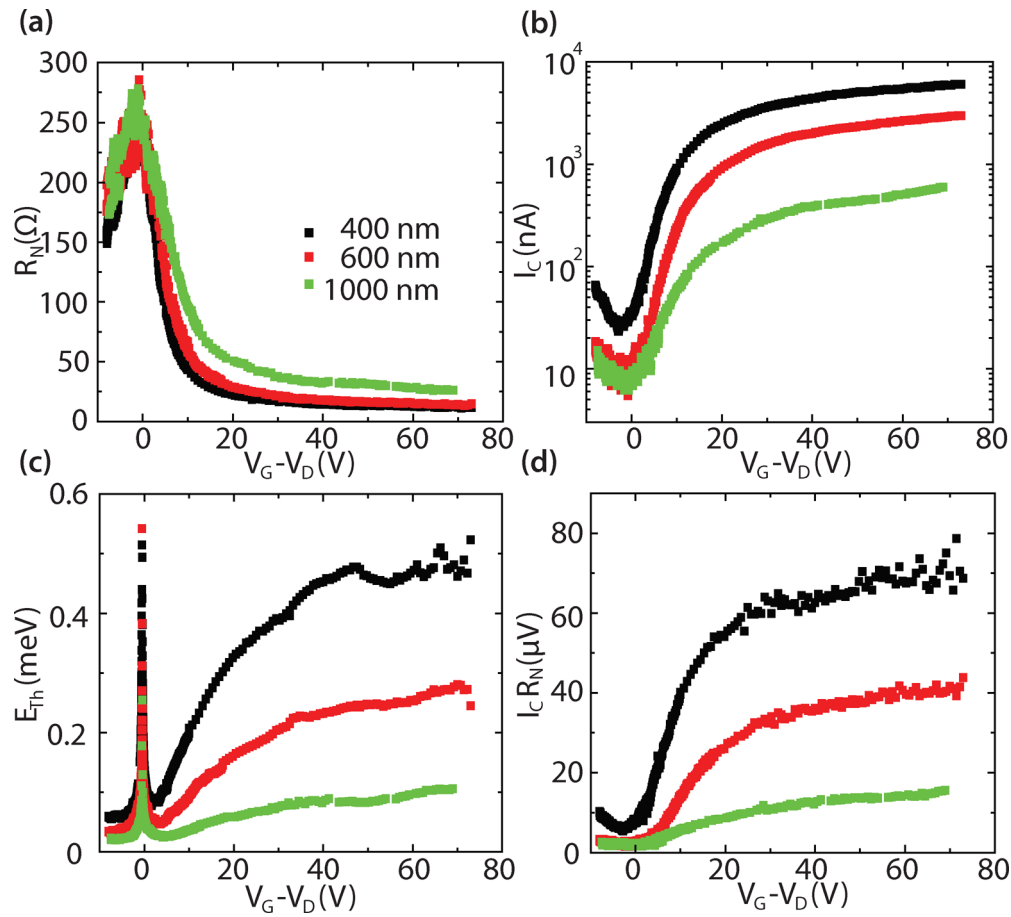
Figure 2. (a) Normal resistance, (b) critical current, (c) calculated Thouless energy, and (d) $I_C R_N$ product, plotted versus the gate voltage measured from the Dirac point, $V_G - V_D$, for the three junctions of different lengths. In panel c, the E_{Th} curves artificially diverge at the DP, because the average density goes to zero while the resistance stays finite. We therefore ignore any data taken with V_G within 7 V from the DP. Outside of this regime, E_{Th} is sufficiently (more than 5 times) larger than $k_B T$, which allows us to use the zero-temperature limit of ref 9. It is clear that the shape and the relative values of the three curves in panel c closely resemble those of panel d, except in the vicinity of the DP.
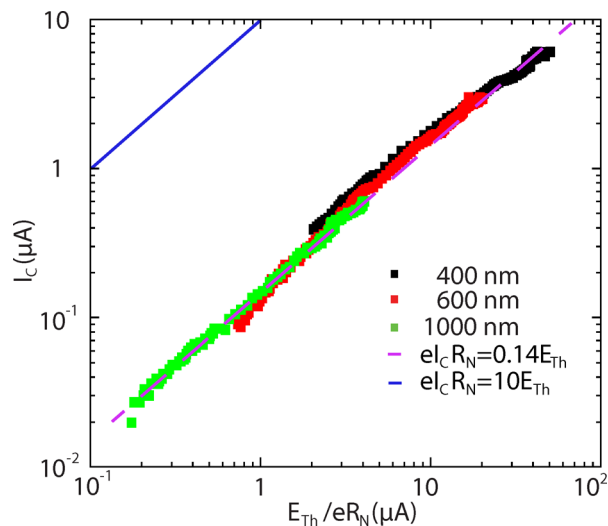

Figure 3. I_C plotted versus E_{Th}/eR_N for the three junctions. Clearly, I_C scales linearly with E_{Th}/eR_N with the same coefficient for the three junctions. However, the proportionality coefficient is suppressed by a factor of 50−100 compared to the theoretical results of ref 9., as discussed in the text. The blue line indicates the expected scaling $eI_C R_N \approx 10E_{Th}$ while the purple fit corresponds to $eI_C R_N = 0.14E_{Th}$.

However, in the Supporting Information we consider different types of graphene-specific material imperfections and estimate, according to ref 23, that these contributions are not enough to explain the observed discrepancy. The reduced value of $eI_C R_N/E_{Th}$ has been previously observed in diffusive graphene-based Josephson junctions[24−26] and attributed to the partial transparency of the contact interface.[25,26] Indeed, in the case of suppressed transmission t, the electron diffusion time inside the junction $\hbar/E_{Th}$ has to be multiplied by the factor of $1/t$ in order to obtain the total dwell time. As a result, E_{Th} would be replaced by tE_{Th} (α being reduced by a factor t).

To account for our observations, t should be ∼0.01−0.02, independent of the junction and the electron density. We consider two interfaces separately, (a) the interface between the metal contact and the graphene underneath, and (b) the interface between the highly doped graphene under the contact and the bulk of graphene outside of the contacts.[27] The transparency of the second interface is conservatively estimated to be much higher than 0.02. For example, at $V_G - V_D = 35$, the number of transversal modes in our junctions is $N \sim 3000$ (including the spin and valley degeneracies.) Transparency of 0.02 would result in a contact resistance of $\frac{h}{e^2}/(tN) \sim 400\Omega$, much larger than the overall normal resistance of either junction (20−40 Ω). Therefore, this highly transparent

interface is unlikely the reason for increasing the dwell time by a factor of almost 100.

On the other hand, graphene under the contact is highly doped and its interface with the contact metal has a much larger number of modes. These modes could have lower transparency, while still yielding a relatively small contact resistance. Furthermore, the gate voltage has relatively little effect on the electron density under the contact; therefore the transparency of the graphene−metal interface should be constant, increasing the dwell time by a gate-independent factor. We therefore identify this interface as a potential reason for the suppressed value of α; clearly further theoretical work is required to substantiate this conjecture.

In summary, we studied the length and density dependence of the critical current in graphene-based Josephson junctions. Away from the Dirac point, the scaling function $eI_C R_N = \alpha E_{Th}$ works well over a range of critical currents covering more than 2 orders of magnitude. However, we observe that $\alpha \sim 0.1-0.2$, instead of $\alpha \sim 10$ as measured in metallic SNS junctions. This suppression may be attributed to the effective enhancement of the electron dwell time in the junction due to the suppressed transmission at the interface between metal and graphene.

■ ASSOCIATED CONTENT

Ⓢ Supporting Information

The Supporting Information is available free of charge on the ACS Publications website at DOI: 10.1021/acs.nanolett.6b00738.

> Additional experimental data, detailed discussion of the transport mechanism in diffusive graphene Josephson junctions, and the switching statistics of junctions.(PDF)

■ AUTHOR INFORMATION

Corresponding Authors
*E-mail: ck92@phy.duke.edu.
*E-mail: gleb@phy.duke.edu.

Notes
The authors declare no competing financial interest.

■ ACKNOWLEDGMENTS

■ REFERENCES

(1) Tinkham, M. *Introduction To Superconductivity*; McGraw-Hill: New York, 1996.

(2) Heersche, H. B.; Jarillo-Herrero, P.; Oostinga, J. B.; Vandersypen, L. M. K.; Morpurgo, A. F. *Nature* **2007**, *446*, 56.

(3) Miao, F.; Wijeratne, S.; Zhang, Y.; Coskun, U. C.; Bao, W.; Lau, C. N. *Science* **2007**, *317*, 1530.

(4) Du, X.; Skachko, I.; Andrei, E. Y. *Phys. Rev. B: Condens. Matter Mater. Phys.* **2008**, *77*, 184507.

(5) Ojeda-Aristizabal, C.; Ferrier, M.; Guéron, S.; Bouchiat, H. *Phys. Rev. B: Condens. Matter Mater. Phys.* **2009**, *79*, 165436.

(6) Calado, V. E.; Goswami, S.; Nanda, G.; Diez, M.; Akhmerov, A. R.; Watanabe, K.; Taniguchi, T.; Klapwijk, T. M.; Vandersypen, L. M. K. *Nat. Nanotechnol.* **2015**, *10*, 761−764.

(7) Shalom, M. Ben; Zhu, M. J.; Fal'ko, V. I.; Mishchenko, A.; Kretinin, A. V.; Novoselov, K. S.; Woods, C. R.; Watanabe, K.; Taniguchi, T.; Geim, A. K.; Prance, J. R. *Nat. Phys.* **2016**, *12*, 318−322.

(8) Amet, F.; Ke, C. T.; Borzenets, I. V.; Wang, J.; Watanabe, K.; Taniguchi, T.; Deacon, R. S.; Yamamoto, M.; Bomze, Y.; Tarucha, S.; Finkelstein, G. *Science* **2016**, *352* (6288), 966−969.

(9) Dubos, P.; Courtois, H.; Pannetier, B.; Wilhelm, F.; Zaikin, A. D.; Schön, G. *Phys. Rev. B: Condens. Matter Mater. Phys.* **2001**, *63*, 064502.

(10) Bointon, T. M.; Barnes, M.; Russo, S.; Craciun, M. F. *Adv. Mater.* **2015**, *27*, 4200.

(11) Li, X.; Cai, W.; An, J.; Kim, S.; Nah, J.; Yang, D.; Piner, R.; Velamakanni, A.; Jung, I.; Tutuc, E.; Banerjee, S. K.; Colombo, L.; Ruoff, R. S. *Science* **2009**, *324* (5932), 1312−1314.

(12) Kim, K. S.; Zhao, Y.; Jang, H.; Lee, S. Y.; Kim, J. M.; Kim, K. S.; Ahn, J.-H.; Kim, P.; Choi, J.-Y.; Hong, B. H. *Nature* **2009**, *457*, 706.

(13) Li, X.; Magnuson, C. W.; Venugopal, A.; Tromp, R. M.; Hannon, J. B.; Vogel, E. M.; Colombo, L.; Ruoff, R. S. *J. Am. Chem. Soc.* **2011**, *133* (9), 2816−2819.

(14) Dhingra, S.; Hsu, J. F.; Vlassiouk, I.; D'Urso, B. *Carbon* **2014**, *69*, 188.

(15) Borzenets, I. V.; Coskun, U. C.; Jones, S. J.; Finkelstein, G. *Phys. Rev. Lett.* **2011**, *107*, 137005.

(16) Borzenets, I. V.; Coskun, U. C.; Jones, S. J.; Finkelstein, G. *IEEE Trans. Appl. Supercond.* **2012**, *22*, 1800104.

(17) Borzenets, I. V.; Coskun, U. C.; Mebrahtu, H. T.; Bomze, Yu. V.; Smirnov, A. I.; Finkelstein, G. *Phys. Rev. Lett.* **2013**, *111*, 027001.

(18) Courtois, H.; Meschke, M.; Peltonen, J. T.; Pekola, J. P. *Phys. Rev. Lett.* **2008**, *101*, 067002.

(19) Castro Neto, A. H.; Guinea, F.; Peres, N. M. R.; Novoselov, K. S.; Geim, A. K. *Rev. Mod. Phys.* **2009**, *81*, 109.

(20) Martin, J.; Akerman, N.; Ulbricht, G.; Lohmann, T.; Smet, J. H.; Klitzing, K.; von Yacoby, A. *Nat. Phys.* **2008**, *4*, 144−148.

(21) Gupta, A. K.; Crétinon, L.; Moussy, N.; Pannetier, B.; Courtois, H. *Phys. Rev. B: Condens. Matter Mater. Phys.* **2004**, *69*, 104514.

(22) Dubos, P.; Courtois, H.; Buisson, O.; Pannetier, B. *Phys. Rev. Lett.* **2001**, *87*, 206801.

(23) Muñoz, W. A.; Covaci, L.; Peeters, F. M. *Phys. Rev. B: Condens. Matter Mater. Phys.* **2015**, *91*, 054506.

(24) Jeong, D.; Choi, J.-H.; Lee, G.-H.; Jo, S.; Doh, Y.-J.; Lee, H.-J. *Phys. Rev. B: Condens. Matter Mater. Phys.* **2011**, *83*, 094503.

(25) Komatsu, K.; Li, C.; Autier-Laurent, S.; Bouchiat, H.; Guéron, S. *Phys. Rev. B: Condens. Matter Mater. Phys.* **2012**, *86*, 115412.

(26) Li, C.; Guéron, S.; Chepelianskii, A.; Bouchiat, H. 2016, arxiv:1602.01489. (Accessed July 11, 2016).

(27) Xia, F.; Perebeinos, V.; Lin, Y.; Wu, Y.; Avouris, P. *Nat. Nanotechnol.* **2011**, *6*, 179−184.